



TITLE:

# Biaxial Fatigue Life Predicted by Crack Growth Analysis in Various Material Microstructures Modeled by Voronoi-Polygons

AUTHOR(S):

Hoshide, Toshihiko

---

CITATION:

Hoshide, Toshihiko. Biaxial Fatigue Life Predicted by Crack Growth Analysis in Various Material Microstructures Modeled by Voronoi-Polygons. Journal of Materials Engineering and Performance 2011, 20(9): 1497-1504

ISSUE DATE:

2011-12

URL:

<http://hdl.handle.net/2433/153030>

RIGHT:

The final publication is available at [www.springerlink.com](http://www.springerlink.com); この論文は出版社版ではありません。引用の際には出版社版をご確認ご利用ください。 ; This is not the published version. Please cite only the published version.

# Biaxial Fatigue Life Predicted by Crack Growth Analysis in Various Material Microstructures Modeled by Voronoi-Polygons

Toshihiko Hoshide<sup>1)</sup>

## 1) Corresponding Author

Department of Energy Conversion Science  
Graduate School of Energy Science, Kyoto University  
Yoshida-Honmachi, Sakyo-ku, Kyoto 606-8501, Japan  
E-mail: toshi.hoshide@ecs.mbox.media.kyoto-u.ac.jp

## Abstract

Fatigue life is affected by the crack growth behavior that depends on the material microstructure as well as the stress biaxiality. By considering such effects on crack growth, a numerical procedure for predicting failure life in biaxial fatigue of materials with different microstructures was proposed in this work. Such a procedure will be helpful in the material design for higher performance of fatigue resistance in a material. The microstructure of a material was first modeled by using Voronoi-polygons, and the crack initiation was analyzed as the result of slip-band formation in individual grains in the modeled microstructure. In the analysis, stress states in individual grains were randomized so that the average stress state should be equivalent to the bulk stress state. An algorithm for the crack growth analysis was established as a competition between the crack-coalescence growth and the propagation as a single crack. The failure life was statistically predicted based on the crack growth behavior simulated for forty distinct microstructural configurations, which were generated by randomizing shapes of Voronoi-polygons for the same material. By applying the proposed procedure, simulations were conducted for experimental conditions of fatigue tests, which had been conducted under axial, torsional and combined loading modes by using circumferentially-notched specimens of pure copper, medium carbon steel, and ( $\alpha+\beta$ ) and  $\beta$  titanium alloys. In this case, forty different failure-lives were obtained for each combination of material and loading mode. It was revealed that the failure lives observed in experiments were almost covered by the life-ranges between the minimum and the maximum lives given in simulation. Statistical characteristics in simulated life-distributions were investigated by using Weibull distribution function and its related statistical parameters.

**Keywords** biaxial fatigue, fatigue crack growth, modeling, material microstructure, Voronoi-polygon, Monte Carlo simulation, life prediction, Statistics

## 1. Introduction

The majority of failures in structural or functional systems are caused by fatigue under biaxial stresses. Based on numerous investigations on fatigue properties under biaxial stresses, several approaches and models have been proposed for the life prediction; i.e., as representative models, a critical plane approach (Ref 1-6), an equivalent strain range approach (Ref 7, 8), a local stress/strain model (Ref 9, 10), an energy model (Ref 11), an event independent cumulative damage model (Ref 12), and so on. Since the actual fatigue damage in structures is caused by the progress of fatigue cracks in them, the fatigue failure life is controlled by cracking behavior, which depends on not only the biaxiality of the applied stress but the material microstructure (Ref 13, 14). Considering that most of dangerous parts in structural components are notched regions, more realistic assessments of failure life of machine or its elements having stress-concentrated parts require a new appropriate procedure based on the analysis of such a crack growth process by reflecting both effects of micro-

structure and stress state. The development of such a procedure is expected to be useful for the material design for higher performance of fatigue resistance in a material. From this point of view, some models of the fatigue process have been proposed to describe the behavior of crack initiation and propagation under biaxial stress state (Ref 15-21). There is, however, no simple model adequately to express geometric features of a complex microstructure of polycrystalline material.

In the present work, an updated analytical procedure is developed based on a previous model (Ref 21) so that it should be more applicable to biaxial fatigue behavior in notched components of materials with different microstructures. Modeling of microstructure in polycrystalline material is especially improved in this investigation, and a microstructure is modeled by using Voronoi-polygons. A new modeling is also introduced in the analysis of crack initiation in a modeled microstructure. Using the developed procedure, a computer simulation of Monte Carlo type is made to clarify the fatigue life in four kinds of materials with different microstructures under axial, torsional and combined axial-torsional loading modes. The applicability of the developed procedure is investigated by comparing simulated results with experimental observations. Statistical characteristics are mainly discussed based on Weibull analysis of simulated failure lives.

## 2. Experimental Fatigue Tests to Be Analyzed

A brief outline of fatigue tests, which will be analyzed by using a proposed procedure, is mentioned at first.

The materials are an oxygen-free pure copper with purity of 99.98%, a medium carbon steel including 0.45wt% C, and two types of Ti-6Al-4V titanium alloys having ( $\alpha+\beta$ ) phases and  $\beta$  phase. Mechanical properties and grain sizes of these materials are summarized in Table 1. Note that there is a large variation especially in grain size.

Specimens were of solid cylindrical type with a circumferential blunt notch as shown in Fig. 1. Table 2 shows the combinations of root radius  $R$  and minimum diameter  $D$  of a notch root, which were employed in experiments of respective materials. For pure copper and medium carbon steel, specimens with two notch-shapes were prepared as shown in Table 2. The fatigue behavior of notched specimens of the four materials had been investigated experimentally in our other works (Ref 17,18, 22).

Fatigue tests were carried out under fully reversed and force-controlled conditions in axial, combined axial-torsional and torsional modes. Fatigue testing conditions to be analyzed are summarized in Table 3. By using the axial stress range  $\Delta\sigma_z$  and the shear stress range  $\Delta\tau_{z\theta}$ , the range of equivalent stress at the notch root,  $\Delta\sigma_{eq}$ , in Table 3 is defined as follows; i.e.,  $\Delta\sigma_{eq} = (\Delta\sigma_z^2 + 4\Delta\tau_{z\theta}^2)^{1/2}$  for pure copper, and  $\Delta\sigma_{eq} = (\Delta\sigma_z^2 + 3\Delta\tau_{z\theta}^2)^{1/2}$  for the other materials. When the equivalent values of von Mises type were applied in describing the cyclic deformation in pure copper, it was revealed that there is no unified relation in the stress vs. plastic-strain behavior between axial and torsional loading. This is the reason why the equivalent stress and plastic-strain of Tresca type are adopted in expressing the cyclic stress-strain relation of pure copper. The constitutive equation of  $\Delta\sigma_{eq} = k (\Delta\varepsilon_{eq})^n$  is obtained from observed cyclic stress-strain curves, and used in a finite element method to analyze elastic-plastic deformation behavior in notched specimens. The material constants  $k$  and  $n$  are respectively  $7.29 \times 10^2 \text{ MPa}$  and 0.116 for pure copper,  $1.73 \times 10^3 \text{ MPa}$  and 0.186 for medium carbon steel,  $3.10 \times 10^3 \text{ MPa}$  and 0.109 for ( $\alpha+\beta$ ) Ti alloy and  $4.36 \times 10^3 \text{ MPa}$  and 0.158 for  $\beta$  Ti alloy.

Since the specimen shape is cylindrical, a cylindrical orthogonal-coordinate  $r-\theta-z$  system is adopted to specify the stress components. The axes of  $\theta$  and  $z$  are respectively set in the circumferential and axial directions of specimen, while the  $r$ -axis coincides with the normal direction of specimen surface.

### 3. Framework of Modeling

In this chapter, the framework of a proposed modeling procedure is described for the transgranular cracking mode by supposing that the fatigue damage may be dominated by the crack growth of transgranular type in the four kinds of materials. Of course, the crack growth modeling for intergranular mode or mixed mode of transgranular and intergranular types is required for materials in which such a complex crack growth becomes predominant for the fatigue damage. In future, an adequate initiation model of intergranular crack should be researched to be able to analyze the initiation life quantitatively, and the modeling of crack growth needs to be improved based on a researched model for crack initiation analysis.

#### 3.1 Modeling of material microstructure by using Voronoi-polygons

It is well known that most of fatigue cracks are initiated on surfaces of stressed elements except for materials in which cracks are initiated from inclusions inside. In this work, the microstructure on the notch root surface of a specimen is modeled as a two-dimensional area by using Voronoi-polygon. A Voronoi diagram is a kind of decomposition of a metric space, which is determined by distances to a specified discrete set of points in the space (Ref 23). It is also known that an aggregate of convex hexagons is obtained as Voronoi-polygons in a two-dimensional Voronoi diagram. The merit in adopting Voronoi-polygons for microstructure of polycrystalline material is that a modeling of microstructure is possible under a simple algorithm in numerical analysis. Since a curved surface of notch root area is developed into a flat surface, i.e., a two-dimensional surface in the present analysis, the circumferential direction ( $\theta$ -direction) of a specimen is developed onto the horizontal direction in the two-dimensional surface when the specimen axis ( $z$ -direction) is set to coincide with the vertical direction.

The size of the aforementioned two-dimensional area is determined as follows. In this case, we should note that the stresses in the region around notch root region decrease when moving away from the notch root in the axial direction. Such a stress gradient and its effects on crack initiation and propagation should be taken into account in the crack growth analysis. For convenience, in this work, the area to be analyzed in this simulation is restricted in the axial direction so that an axial or shear stress generated on the surface of the notch area must exceed at least 95% of the maximum stress at the notch root. Finally, sizes in the circumferential ( $\theta$ ) direction and in the axial ( $z$ ) direction are set depending on material and notch geometry as shown in Table 4.

The number of polygons,  $n$ , in the analyzed area is determined so that the resultant mean grain-size should approximately equal the size measured in experiment. The polygon-number for a material consisting of one phase, such as pure copper or  $\beta$  Ti alloy, is determined by the just-above mentioned procedure.

On the other hand, medium carbon steel consists of ferrite and pearlite grains, and ( $\alpha+\beta$ ) Ti alloy has  $\alpha$ - and  $\beta$ -phase grains in its microstructure. For these materials, Voronoi-polygons are randomly selected among all Voronoi-polygons so that an area-rate of selected polygons occupying in the analyzed area could coincide with the microstructural composition observed in a material under consideration. In medium carbon steel, by setting the area-rate to be 0.27, which is experimentally observed in medium carbon steel, the resultantly selected polygons are regarded as pearlite grains. In ( $\alpha+\beta$ ) Ti alloy, grains of  $\beta$ -phase are observed to be larger than that of  $\alpha$ -phase. Therefore, for ( $\alpha+\beta$ ) Ti alloy, Voronoi-polygons are randomly selected, and each extracted Voronoi-polygon is treated as the polygon that nucleates  $\beta$ -phase. Then, the neighboring two Voronoi-polygons for a selected polygon nucleating  $\beta$ -phase are clustered into one polygon. The clustered polygon is regarded as a final  $\beta$ -phase grain. This process is iterated so that the area-rate of  $\beta$ -phase

grains occupying in the analyzed area should be 0.42, which is experimentally observed in ( $\alpha+\beta$ ) Ti alloy.

Polygons formed as mentioned above are hereafter called grains, which constitutes polycrystalline material. Figure 2 shows an example of modeled microstructure.

### 3.2 Stress state in modeled grain and grain size

Since individual grains have differences in geometrical shape and deformation response in an actual polycrystalline material, a stress state in one grain is supposed to differ from that in another grain as illustrated in Fig. 3. Therefore, it is reasonable to consider that stresses, to which individual grains are subjected, are different from the applied bulk stress. The present model assumes that stress states in individual grains deviate from the given applied stress state in the crack initiation analysis as follows.

$$\Delta\sigma_z^{(i)} = \Delta\sigma_z f_i, \Delta\sigma_\theta^{(i)} = \Delta\sigma_\theta g_i, \text{ and } \Delta\tau_{z\theta}^{(i)} = \Delta\tau_{z\theta} h_i \quad (1)$$

In Eq. (1),  $\Delta\sigma_z$ ,  $\Delta\sigma_\theta$  and  $\Delta\tau_{z\theta}$  are respectively axial, hoop and shear stress range components of the applied bulk stress, and  $\Delta\sigma_z^{(i)}$ ,  $\Delta\sigma_\theta^{(i)}$  and  $\Delta\tau_{z\theta}^{(i)}$  are the stress range components in the  $i$ -th grain as shown in Fig. 3. These stress ranges are defined in the aforementioned  $r$ - $\theta$ - $z$  coordinate system. Deviation factors  $f_i$ ,  $g_i$  and  $h_i$  in Eq. (1) are randomly given within the range from 0.5 to 1.5 so that they should satisfy the condition specified in Eq. (2).

$$\sum_{i=1}^n f_i / n = 1, \sum_{i=1}^n g_i / n = 1, \text{ and } \sum_{i=1}^n h_i / n = 1 \quad (2)$$

In Eq. (2),  $n$  is the aforementioned number of grains set in the analyzed area. Equation (1) under the condition of Eq. (2) implies that stress states in individual grains are randomized so that the average stress state should be equivalent to the bulk stress state. For the simplicity in application, in this work, a uniform distribution is assumed in expressing the variation of stress state in an individual grain. In spite of such a simple assumption, it is elucidated that the distribution of crack initiation angle is adequately simulated under the aforementioned assumption in biaxial fatigue (Ref 24).

The grain size is defined as the length of line-segment passing through the nucleus-point in a Voronoi-polygon as illustrated in Fig. 3. In the following analysis of crack initiation, the grain size  $d^{(i)}$  of the  $i$ -th grain will be also used as the slip-band length in the grain.

### 3.3 Competition model for fatigue crack growth under biaxial stresses

A competition model for crack growth established by the authors (Ref 15, 16, 18, 21) is also applied in this simulation. The model postulates that the cracking morphology and the fatigue failure life are determined as the result of competition between the growth by crack coalescence and the propagation of a main crack as a single crack. The competition implies that the dominant crack growth will be governed by the faster growth mode. Each analytical procedure is summarized in the following.

#### 3.3.1 Crack initiation analysis

In the crack initiation analysis too, the  $r$ - $\theta$ - $z$  coordinate system is employed as depicted in Fig. 4. The  $z$ -axis is set to be parallel to the axial direction of specimen. Consider a slip plane in one grain on the specimen surface. On the slip plane, another orthogonal  $\xi$ - $\eta$ - $\zeta$  coordinate system is also defined so that the  $\xi$ - and  $\eta$ - axes should be respectively parallel to the normal direction of the slip plane and the slip direction on the slip plane.

The stress component  $[\sigma_{\xi\eta\zeta}]$  for the slip system is correlated with an applied stress  $[\sigma_{r\theta z}]$  as Eq. (3), by using the directional cosine  $[l]$  which is defined between  $r$ - $\theta$ - $z$  and  $\xi$ - $\eta$ - $\zeta$  coordinates.

$$[\sigma_{\xi\eta\zeta}] = [l] [\sigma_{r\theta z}] [l]^T, \text{ and } [l] = \begin{bmatrix} l_{r\xi} & l_{r\eta} & l_{r\zeta} \\ l_{\theta\xi} & l_{\theta\eta} & l_{\theta\zeta} \\ l_{z\xi} & l_{z\eta} & l_{z\zeta} \end{bmatrix} \quad (3)$$

In the above equation, the superscript “T” represents the transposed matrix,

$$[\sigma_{r\theta z}] = \begin{bmatrix} \sigma_r & \tau_{r\theta} & \tau_{rz} \\ \tau_{\theta r} & \sigma_\theta & \tau_{\theta z} \\ \tau_{zr} & \tau_{z\theta} & \sigma_z \end{bmatrix}, \text{ and } [\sigma_{\xi\eta\zeta}] = \begin{bmatrix} \sigma_\xi & \tau_{\xi\eta} & \tau_{\xi\zeta} \\ \tau_{\eta\xi} & \sigma_\eta & \tau_{\eta\zeta} \\ \tau_{\zeta\xi} & \tau_{\zeta\eta} & \sigma_\zeta \end{bmatrix} \quad (4)$$

Considering slip in a surface grain, we may assume the plane stress state as  $\sigma_r = \tau_{rz} = \tau_{zr} = \tau_{r\theta} = \tau_{\theta r} = 0$ . Under the above assumption, the resolved shear stress  $\tau_{\xi\eta}$  in the slip direction on the associated slip plane, which is one of the most important factors for the feasibility to slip, is represented by

$$\tau_{\xi\eta} = \sigma_z l_{z\eta} l_{\theta\eta} + \sigma_\theta l_{z\xi} l_{\theta\xi} + \tau_{z\theta} (l_{z\xi} l_{\theta\eta} + l_{z\eta} l_{\theta\xi}) \quad (5)$$

As illustrated in Fig. 4, the angle  $\phi$  of slip-band is defined counterclockwise against the  $\theta$  axis on the specimen surface, and is calculated as follows.

$$\phi = \arctan (-l_{\theta\xi} / l_{z\xi}) \quad (6)$$

In this model, a crack is assumed to be initiated along the slip band when the criterion,  $\tau_{\xi\eta} \geq \tau_c$  in which  $\tau_c$  is the critical shear stress to make a slip active, is satisfied, and also the number of stress cycles,  $N_i$ , which is required to make a slip band into a crack, has passed. The parameter  $N_i$  is identical to the crack initiation life, and is calculated by using a dislocation pile-up model (Ref 25) as

$$N_i = \frac{2GW_c}{\pi(1-\nu)d(\tau_{\xi\eta} - \tau_c)^2} \quad (7)$$

In Eq. (7), material constants  $G$ ,  $\nu$  and  $W_c$  are respectively the shear elastic modulus, Poisson's ratio and the fracture surface-energy, all of which are material constants. The parameter  $d$  is the slip band length in a grain to be considered in the slip analysis.

### 3.3.2 Crack propagation analysis

The mode of crack propagation is analyzed presuming that the growth rate  $da/dN$  is expressed by a power function of the  $J$ -integral range,  $\Delta J$ , as follows.

$$\frac{da}{dN} = C \Delta J^m \quad (8)$$



In Eq. (8),  $C$  and  $m$  are material constants.  $J$ -integral range is evaluated assuming that short surface-cracks are semi-circular. The evaluation of  $J$ -integral range for short surface-cracks is given elsewhere (Ref 26, 27). The propagation life required for a given crack extension can be calculated by integrating Eq. (8) with respect to the crack length. The integral calculation is also employed in determining the time at which a subsequent crack linkage occurs, or the failure life which is calculated for a given crack length.

### 3.3.3 Crack coalescence analyses

During the crack initiation and propagation stages, the coalescence growth is taken into account among distributed cracks, or propagating cracks. In the crack initiation stage, a newly initiated crack is assumed to link with one of previously initiated cracks, if the tip-to-tip distance between the cracks (see Fig. 5) is less than a specific length  $\xi d_0$ . The size  $d_0$  is the mean grain size for the modeled microstructure. The coalescence in the crack propagation stage is presumed to occur when the tip-to-tip distance between the main and the secondary cracks (see Fig. 6) becomes less than  $\zeta d_0$ . The values of  $\xi$  and  $\zeta$ , which depend on the combination of material microstructure and loading mode, are determined according to experimental observations. Larger value of  $\xi$  or  $\zeta$  implies that cracks can more easily coalesce together. When one of tips of a crack reaches a boundary of the analyzed area, the growth analysis for the crack is discontinued.

## 4. Simulation and Discussion

### 4.1 Simulation procedure

Table 5 summarizes values of parameters used in the simulation for each material and respective loading mode. As for the fracture surface-energy  $W_c$ , the energy absorbed due to plastic deformation is employed in calculating  $W_c$ -value according to the energy criterions (Ref 28, 29). Plastic deformation energy is known to be about  $10^3$  to  $10^4$  times greater than the surface energy, which is given for each materials (Ref 30). In this work,  $10^4$  as the multiplication factor to the surface energy is adopted for pure copper which has larger work-hardening, while  $10^3$  is used as the multiplication factor for the other materials which have less work-hardening. The critical shear stress  $\tau_c$  is evaluated as the shear stress giving long-life data near the fatigue limit, which has been estimated from experimental results in pure torsional tests for pure copper and medium carbon steel and in rotating bending tests for Ti alloys (Ref 31). The parameters  $C$  and  $m$  in Eq. (8) are obtained based on the behavior of small crack growth, which have been observed in fatigue tests using smooth tubular specimens in axial, combined axial-torsional and torsional loading-modes under strain-controlled condition. The values of  $C$  and  $m$  in Table 5 are given for  $da/dN$  in m/cycle and  $\Delta J$  in  $J/m^2$ . However, it is difficult to estimate the coalescence parameters  $\xi$  and  $\zeta$  for lack of experimental observations concerning more various materials and loading modes. Therefore, the parameters  $\xi$  and  $\zeta$  have been determined based on actual crack coalescence behavior observed in experiment (Ref 32).

By desktop computer, numerical simulations for the fatigue testing conditions as above-mentioned were executed by using a Monte Carlo type procedure. Employing forty series of uniform random numbers, forty distinct modeled microstructures are generated for a material. Such forty microstructures are respectively composed of different-shaped grains and have distinct combinations of directions of slip-lines and slip-planes in the individual grains. The crack growth under each condition of fatigue testing is analyzed in respective microstructure generated for the material.

### 4.2 Comparison of simulated results with experimental ones

Forty distinct cracking patterns can be finally obtained for each material under a given condition of fatigue testing through Monte Carlo simulations. It is confirmed that the feature of the cracking morphology and its dependence on the stress state, which had been observed experimentally (Ref 17, 18, 22), are adequately simulated by using the proposed procedure. By monitoring cracking behavior during a simulation, a crack growth curve is given as the relation between the number of cycles and the length of main crack for a material subjected to a specified loading mode. Such a crack growth curve enables us to determine the failure life defined by a prescribed crack length.

The failure life  $N_f$  in experiments is defined as the number of cycles at which a dominant crack of a specific length is formed at the notched portion. The crack length is prescribed according to experimental observations (Ref 17, 18, 22). In simulations, the failure life is calculated as the formation cycles leading to the dominant crack with a specific length for consistency with the experiment of each material. The specific crack lengths are respectively 2mm for pure copper, 1mm for medium carbon steel, 0.3mm for  $(\alpha+\beta)$  Ti alloy, and 3mm for  $\beta$  Ti alloy. Figure 7 shows the comparison between the actual failure life observed in experiments and the simulated life. In the figure, each symbol presents a data point of the actual life correlated with the average of forty lives simulated for the corresponding material under one testing condition. Two dotted-straight lines in Fig. 7 present factors of two in the life dispersion. It is found that the predicted life-ranges almost cover actual failure lives in experiments. Although the data simulated for  $(\alpha+\beta)$  Ti alloy under torsional loading appear to shift toward longer life region, such a deviation gives a conservative estimation. Considering a possible scatter of failure life to appear in experiments, it may be generally concluded that the proposed procedure gives a good estimation for the failure life in materials with various microstructures under biaxial fatigue.

#### 4.3 Statistical properties of simulated lives

It is difficult that a statistical distribution of failure life is investigated experimentally, because many experiments are required for a given condition of biaxial fatigue testing. It is clarified that a reasonable life prediction is possible by using the proposed procedure in a previous section. In this section, statistical properties of life distribution are discussed by using life-distributions simulated by using the proposed procedure. In this work, a distribution of simulated lives for respective fatigue condition is fitted to the three-parameter Weibull distribution function expressed as

$$F(N_f) = 1 - \exp \left[ - \left( \frac{N_f - N_L}{N_S} \right)^\alpha \right] \quad (9)$$

The three parameters,  $\alpha$ ,  $N_S$  and  $N_L$ , in the above equation are respectively the shape, scale and location parameters.

Simulations under the combinations of material, loading mode and notch root radius, result in 42 life-distributions in total. It is found that 36 distributions among them are well fitted to the three-parameter Weibull distribution function of Eq. (9), though we cannot see a good approximation for the remaining 6 life-distributions. The location parameter  $N_L$  in the three-parameter Weibull distribution function implies the minimum life in the fitted life-distribution. Figure 8 presents the observed actual failure-life correlated with the location parameter  $N_L$  in the 36 life-distributions, which can be approximated by Eq. (9). As seen in Fig. 8, the location parameter gives a conservative estimation for the failure life.

In the following, a life scatter is discussed in correlation with loading mode. The life scatter to be discussed is represented by the coefficient of variation COV, and the shape



parameter  $\alpha$  in the two-parameter Weibull distribution function. The parameter COV is defined as the standard deviation of simulated lives divided by the average life, and the two-parameter Weibull distribution function is given as the distribution function setting  $N_L = 0$  in Eq. (9). Of course, a larger COV-value implies a larger scatter of life. The parameter  $\alpha$  corresponds to the inclination in the relation expressed by a straight line in Weibull probability paper. A larger  $\alpha$ -value means a steeper inclination in the approximated relation of life distribution, i.e., a smaller scatter. Figure 9 presents dependencies of the two parameters on the loading mode. Although values of COV and  $\alpha$  themselves have large scatters, their dependencies on loading mode are seen somewhat. Such a dependency on loading mode, however, is quite different in the four materials. When a torsional component increases in loading mode, the life scatter becomes larger in pure copper and  $\beta$  Ti alloy as seen in Figs. 9(a) and (d), but smaller in  $(\alpha+\beta)$  Ti alloy as seen in Fig. 9(c). On the other hand, as for medium carbon steel, the largest scatter seems to appear in the combined loading mode as seen in Fig. 9(b). The difference in loading-mode dependency may be ascribed to the crack growth behavior affected by the combination of material microstructure and loading mode. In future, this issue should be clarified by more detailed investigation on the mutual correspondence among cracking behavior, material microstructure and loading mode.

## 5. Conclusions

In the present work, a model of fatigue crack growth under biaxial stresses was developed to simulate cracking behavior and to evaluate failure life for notched components. In modeling, an aggregate of Voronoi-polygons was adopted to express microstructural features of a polycrystalline material adequately. An algorithm for the crack growth in the microstructure modeled by using Voronoi-polygons was established as a competition between the growth by crack coalescences and the propagation of a dominant crack as a single crack. The coalescence growth under the assumed criteria was taken into account among initiated and/or propagating cracks during the whole fatigue process.

The failure life was defined as the number of cycles required for the formation of crack, which had a specific length, and the life was estimated by using the proposed procedure combined with simulations of Monte Carlo type. Simulated results were compared with experimental observations in previous fatigue tests of circumferentially notched specimens, which had been carried out using pure copper, medium carbon steel, and  $(\alpha+\beta)$  and  $\beta$  Ti alloys under axial, combined axial and torsional, torsional loading. Forty trials of simulations were conducted for each material under a given loading mode. Such simulations brought forty different failure lives, which were defined as the number of cycles to the formation of dominant crack with a specified length. Simulated life-ranges from the minimum to the maximum lives were found to cover the failure life observed in experiments. Statistics of simulated lives was also discussed based on a Weibull statistical analysis. It was clarified that the location parameter in fitted three-parameter Weibull distribution function gave conservative life assessment.

## Acknowledgments

A part of this work was supported by Grant-in-Aids for Scientific Research (C) from Japan Society for Promotion of Science. The author also wishes to thank Mr. Sata, Mr. Takahashi, Mr. Kasai and Mr. Adachi, who were previous students of Kyoto University, for taking charge of part of this work.

## References

1. J. Dasa, and S.M. Sivakumarb, An Evaluation of Multiaxial Fatigue Life Assessment Methods for Engineering Components, *Int. J. Press. Vessels Piping*, 1999, **76**, p 741-746

2. J. Dasa, and S.M. Sivakumarb, Multiaxial Fatigue Life Prediction of a High Temperature Steam Turbine Rotor Using a Critical Plane Approach, *Eng. Failure Analysis*, 2000, **7**, p 347-358
3. U. Kocabicak, and M. Firat, A Simple Approach for Multiaxial Fatigue Damage Prediction Based on FEM Post-Processing, *Mater Design*, 2004, **25**, p 73-82
4. L. Reis, B. Li, M. Leite M, and M. de Freitas, Effects of Non-Proportional Loading Paths on the Orientation of Fatigue Crack Path, *Fatigue Fract. Eng. Mater. Struct.*, 2005, **28**, p 445-454
5. A. Varvani-Farahani, T. Kodric, and A. Ghahramani, A Method of Fatigue Life Prediction in Notched and Un-Notched Components, *J. Mater. Process. Technol.*, 2005, **169**, p 94-102
6. X. Chen, J. Song, and K.S. Kim, Low Cycle Fatigue Life Prediction of 63Sn–37Pb Solder under Proportional and Non-Proportional Loading, *Int. J. Fatigue*, 2006, **28**, p 757-766
7. L. Reis, B. Li, and M. de Freitas, Biaxial Fatigue for Proportional and Non-Proportional Loading Paths, *Fatigue Fract. Eng. Mater. Struct.*, 2004, **27**, p 775-784
8. B. Li, L. Reis, and M. de Freitas, Simulation of Cyclic Stress/Strain Evolutions for Multiaxial Fatigue Life Prediction, *Int. J. Fatigue*, 2006, **28**, p 451-458
9. N. Hong, and L. Shaobo, Biaxial Stress Fatigue Life Prediction by the Local Strain Method, *Int. J. Fatigue*, 1997, **19**(6), p 517-522
10. G.Q. Sun, and D.G. Shang, Prediction of Fatigue Lifetime under Multiaxial Cyclic Loading Using Finite Element Analysis, *Mater Design*, 2010, **31**, p 126-133
11. G. Gasiak, and R. Pawliczek, Application of an Energy Model for Fatigue Life Prediction of Construction Steels under Bending, Torsion and Synchronous Bending and Torsion, *Int. J. Fatigue*, 2003, **25**, p 1339-1346
12. Y. Jiang, W. Ott, C. Baum, M. Vormwald, and H. Nowack, Fatigue Life Predictions by Integrating EVICD Fatigue Damage Model and an Advanced Cyclic Plasticity Theory, *Int. J. Plasticity*, 2009, **25**, p 780-801
13. C. T. Hua, and D.F. Socie, Fatigue Damage in 1045 Steel under Variable Amplitude Biaxial Loading. *Fatigue Fract. Eng. Mater. Struct.*, 1985, **8**, p 101-114
14. J.A. Bannantine, and D.F. Socie, Observations of Cracking Behavior in Tension and Torsion Low Cycle Fatigue, *ASTM STP 942*, 1988, p 899-921.
15. T. Hoshide, and D.F. Socie, Crack Nucleation and Growth Modeling in Biaxial Fatigue, *Eng. Fract. Mech.*, 1988, **29**(3), p 287-299
16. T. Hoshide, T. Kawabata, and T. Inoue, Analysis of Intergranular Cracking in Low Cycle Fatigue under Biaxial Stresses, *Trans. Jpn Soc. Mech. Engrnr, Ser. A*, 1989, **55**(510), p 222-230
17. T. Hoshide, K. Yokota, and T. Inoue, Investigation on Small Crack Growth and Life Predictions in Fatigue of Circumferentially-Notched Component of Pure Copper Subjected to Combined Loading, *J. Soc. Mater. Sci., Jpn*, 1990, **39**(437), p 144-149
18. T. Hoshide, and T. Inoue, A Modeling of Cracking Behavior in Multiaxial Loading, *Proc 4th Int Conf Fatigue and Fatigue Thresholds, Fatigue '90*, Ed. by H. Kitagawa, and T. Tanaka, 1990, **IV**, p 2161-2166
19. T. Argence, J. Weiss, and A. Pineau, Observation and Modelling of Transgranular and Intergranular Multiaxial Low-Cycle Fatigue Damage of Austenitic Stainless Steel, *Multiaxial Fatigue and Design*, Ed. by A. Pineau, G. Cailletaud, and T.C. Lindley, Mechanical Engineering Publications, UK, 1996, p 209-227
20. D.F Socie, and S. Furman, Fatigue Damage Simulation Models for Multiaxial Loading, *Proc. 6th Int. Conf. Fatigue Congress, Fatigue '96*, Ed. by G. Lütjering, and H. Nowack, 1996, **II**, p 967-976

21. T. Hoshide, and T. Kusuura, Life Prediction by Simulation of Crack Growth in Notched Components with Different Microstructures and under Multiaxial Fatigue, *Fatigue Fract. Eng. Mater. Struct.*, 1998, **21**(2), p 201-213
22. T. Hoshide, T. Hirota, and T. Inoue, Fatigue Behavior in Notched Component of ( $\alpha+\beta$ ) and  $\beta$  Titanium Alloys under Combined Axial-Torsional Loading, *Mater. Sci. Res. Int.*, 1995, **1**(3), p 169-174
23. A. Okabe, B. Boots, K. Sugihara, and S.N. Chiu, *Spatial Tessellations - Concepts and Applications of Voronoi Diagrams*, 2nd ed., Chichester, John Wiley, 2000
24. T. Hoshide, and Y. Takahashi, Simulation of Directional Distribution of Slip-Band Crack under Biaxial Low Cycle Fatigue, *JSME International Journal, Ser. A*, 2004, **47**(3), p 397-402
25. K. Tanaka, and T. Mura, A Dislocation Model for Fatigue Crack Initiation, *Trans. ASME, J. Appl. Mech.*, 1981, **48**, p 97-103
26. T. Hoshide, T. Yamada, S. Fujimura, and T. Hayashi, Short Crack Growth and Life Prediction in Low-Cycle Fatigue of Smooth Specimens, *Eng. Fract. Mech.*, 1985, **21**(1), p 85-101
27. T. Hoshide, and D.F. Socie, Mechanics of Mixed Mode Small Fatigue Crack Growth, *Eng. Fract. Mech.*, 1987, **26**(6), p 841-850
28. E. Orowan, Fundamentals of Brittle Behavior in Metals, Ed. W.M. Murray, *Fatigue and Fracture of Metals*, MIT Press and John Wiley and Sons Inc, NY, 1952, p 139-167
29. G.R. Irwin, Fracture Dynamics, *Trans. ASME*, 1948, **40A**, p 147-166
30. L.E. Murr, *Interfacial Phenomena in Metals and Alloys*, Addison-Wesley Publ Co, London, 1975, p 124-131
31. The Society of Materials Science, Japan, *Databook on Fatigue Strength of Metallic Materials*, Elsevier Science BV, Amsterdam, 1996, p 644-1763
32. T. Hoshide, M. Miyahara, and T. Inoue, Life Prediction Based on Analysis of Crack Coalescence in Low Cycle Fatigue, *Eng. Fract. Mech.*, 1987, **27**(1), p 91-101

Table 1 Physical properties of materials to be analyzed

| Material                    | Yield strength, $\sigma_y$ | Elongation, $\varphi$ | Young's modulus, $E$ | Poisson's ratio, $\nu$ | Mean grain size, $d_o$ |
|-----------------------------|----------------------------|-----------------------|----------------------|------------------------|------------------------|
| Pure copper                 | 83MPa                      | 80%                   | 139GPa               | 0.37                   | 55 $\mu$ m             |
| Medium carbon steel         | 410MPa                     | 38%                   | 206GPa               | 0.23                   | 21 $\mu$ m             |
| ( $\alpha+\beta$ ) Ti alloy | 911MPa                     | 19%                   | 110GPa               | 0.35                   | 8.5 $\mu$ m            |
| $\beta$ Ti alloy            | 849MPa                     | 6.8%                  | 127GPa               | 0.41                   | 400 $\mu$ m            |

Table 2 Radius  $R$  and minimum diameter  $D$  of notch root

| Material                                        | Radius, $R$ | Minimum diameter, $D$ |
|-------------------------------------------------|-------------|-----------------------|
| Pure copper                                     | 5mm         | 14mm                  |
| Medium carbon steel                             | 3mm         | 15mm                  |
| ( $\alpha+\beta$ ) Ti alloy<br>$\beta$ Ti alloy | 6mm         | 8mm                   |

Table 3 Fatigue testing conditions

| Material                    | Range of equivalent stress, $\Delta\sigma_{eq}$ (MPa) | Ratio of shear stress to axial stress, $\Delta\tau_z/\Delta\sigma_z$ |
|-----------------------------|-------------------------------------------------------|----------------------------------------------------------------------|
| Pure copper                 | 388, 465                                              | 0, 1.5, $\infty$                                                     |
| Medium carbon steel         | 1000, 1200                                            | 0, 1.5, $\infty$                                                     |
| ( $\alpha+\beta$ ) Ti alloy | 1800, 2000, 2200                                      | 0, 1.73, $\infty$                                                    |
| $\beta$ Ti alloy            | 1700, 1900, 2100                                      | 0, 1.73, $\infty$                                                    |

Table 4 Ranges in  $z$ - and  $\theta$ -axes in analyzed area

| Material              |                | Pure copper |       | Medium carbon steel |       | ( $\alpha+\beta$ ) Ti alloy | $\beta$ Ti alloy |
|-----------------------|----------------|-------------|-------|---------------------|-------|-----------------------------|------------------|
| Notch root radius $R$ |                | 3mm         | 5mm   | 3mm                 | 5mm   | 6mm                         | 6mm              |
| Area size             | $z$ -axis      | 1.2mm       | 1.5mm | 1.2mm               | 1.5mm | 0.4mm                       | 3mm              |
|                       | $\theta$ -axis | 3.2mm       | 3.2mm | 1.5mm               | 1.5mm | 0.4mm                       | 6mm              |
| Number of grains, $n$ |                | 846         | 1034  | 1620                | 2025  | 2209                        | 110              |

Table 5 List of parameters used in simulations

| Parameter                  |                | Pure copper            | Medium carbon steel    | ( $\alpha+\beta$ ) Ti alloy | $\beta$ Ti alloy       |
|----------------------------|----------------|------------------------|------------------------|-----------------------------|------------------------|
| $W_c$ (kJ/m <sup>2</sup> ) |                | 6.25                   | 2.0                    | 2.0                         | 2.0                    |
| $\tau_c$ (MPa)             |                | 26                     | 108                    | 288                         | 296                    |
| $C$                        | Mode I         | $4.18 \times 10^{-13}$ | $1.61 \times 10^{-13}$ | $1.07 \times 10^{-10}$      | $7.03 \times 10^{-12}$ |
|                            | Combined mode  | $4.18 \times 10^{-13}$ | $1.61 \times 10^{-13}$ | $1.10 \times 10^{-10}$      | $1.89 \times 10^{-10}$ |
|                            | Mode II        | $4.18 \times 10^{-13}$ | $8.66 \times 10^{-11}$ | $3.91 \times 10^{-15}$      | $3.86 \times 10^{-11}$ |
| $m$                        | Mode I         | 1.69                   | 1.68                   | 1.12                        | 1.32                   |
|                            | Combined mode  | 1.69                   | 1.68                   | 0.96                        | 0.84                   |
|                            | Mode II        | 1.69                   | 0.88                   | 1.74                        | 0.82                   |
| $\xi$                      | Axial mode     | 0.85                   | 0.85                   | 1.7                         | 0.17                   |
|                            | Combined       | 0.85                   | 0.17                   | 1.7                         | 0.09                   |
|                            | Torsional mode | 0.85                   | 0.17                   | 1.7                         | 0.09                   |
| $\zeta$                    | Axial mode     | 0.8                    | 7.0                    | 3.5                         | 1.75                   |
|                            | Combined       | 0.8                    | 4.0                    | 3.5                         | 0.88                   |
|                            | Torsional mode | 0.7                    | 4.0                    | 3.5                         | 0.88                   |

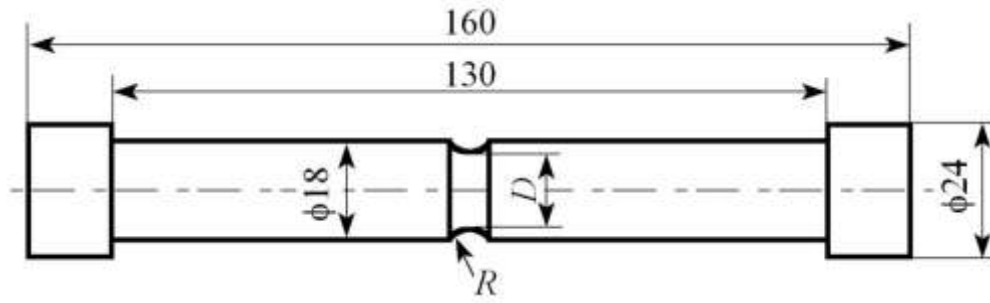


Fig. 1 Specimen used in fatigue tests

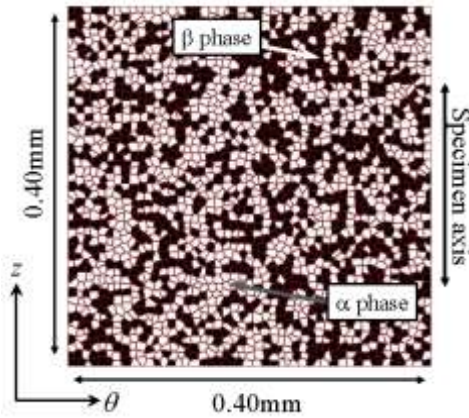


Fig. 2 Example of (α+β) Ti alloy microstructure modeled by using Voronoi-polygons

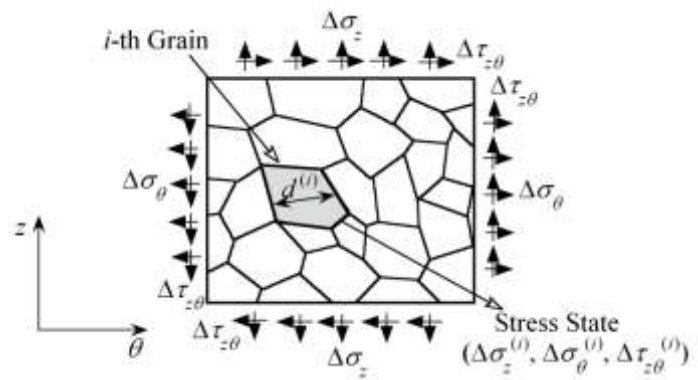


Fig. 3 Schematic illustration of grain-structure and stress state in *i*-th grain

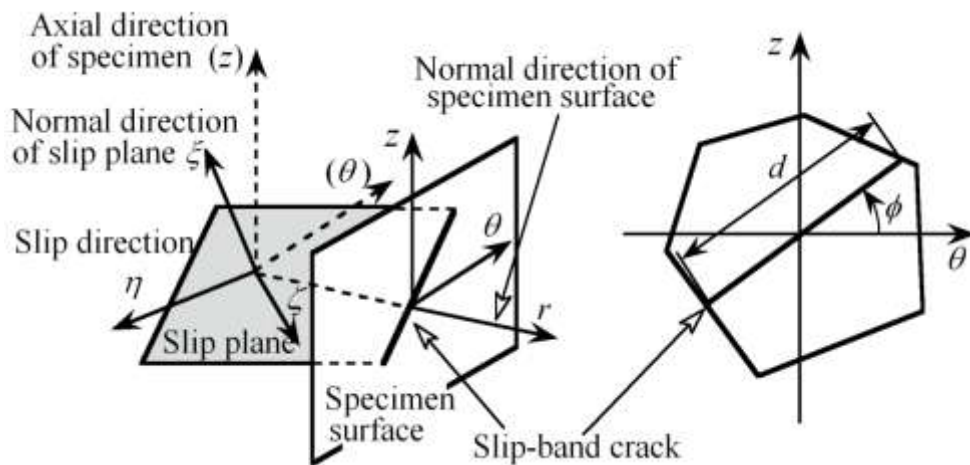


Fig. 4 Geometric relation of slip plane to specimen surface, and direction of slip-band crack



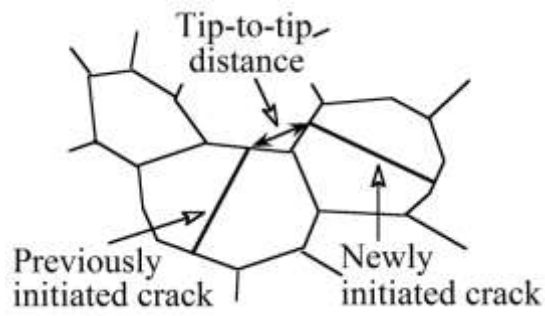


Fig. 5 Coalescence analysis in initiation stage

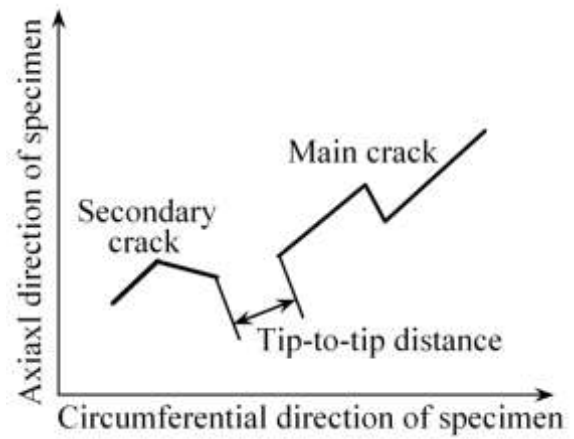


Fig. 6 Coalescence analysis in propagation stage

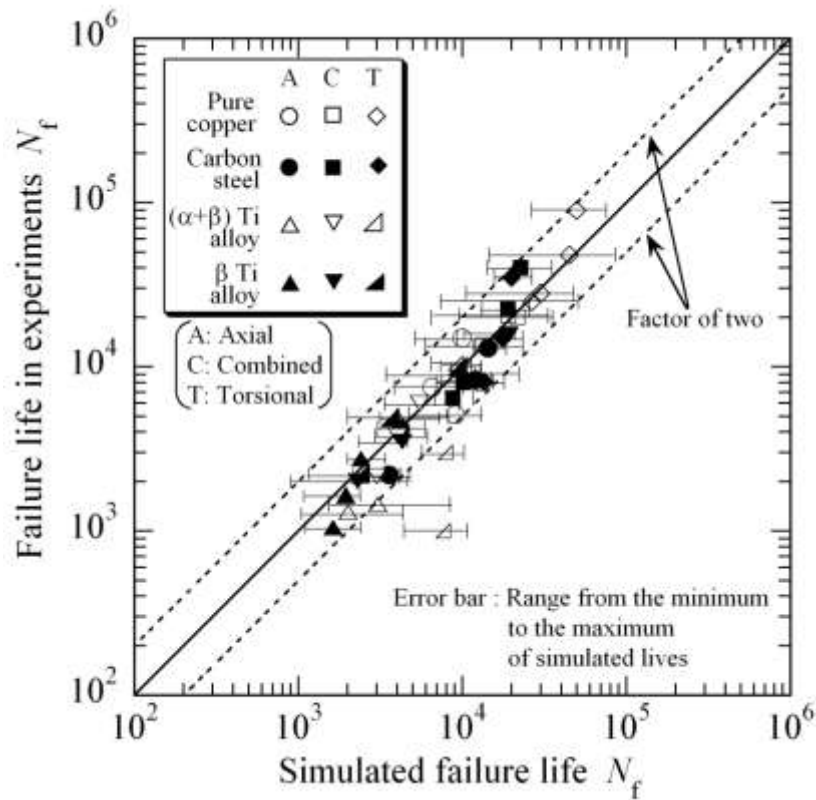


Fig. 7 Comparison between simulated and experimental failure life

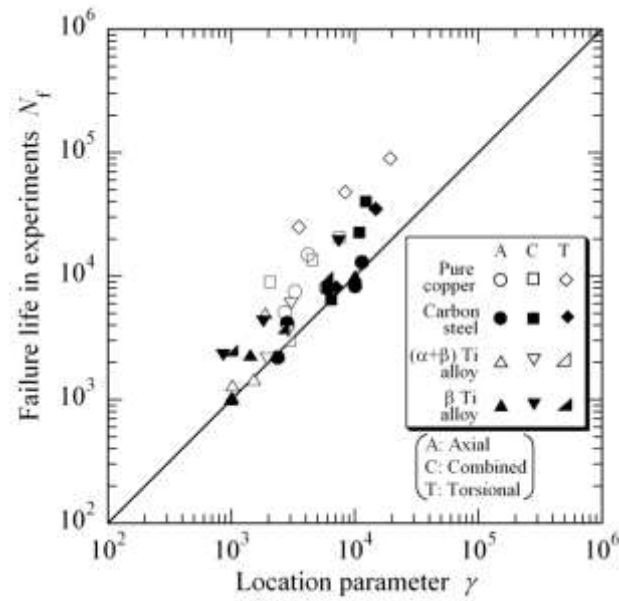


Fig. 8 Correlation of failure life to location parameter

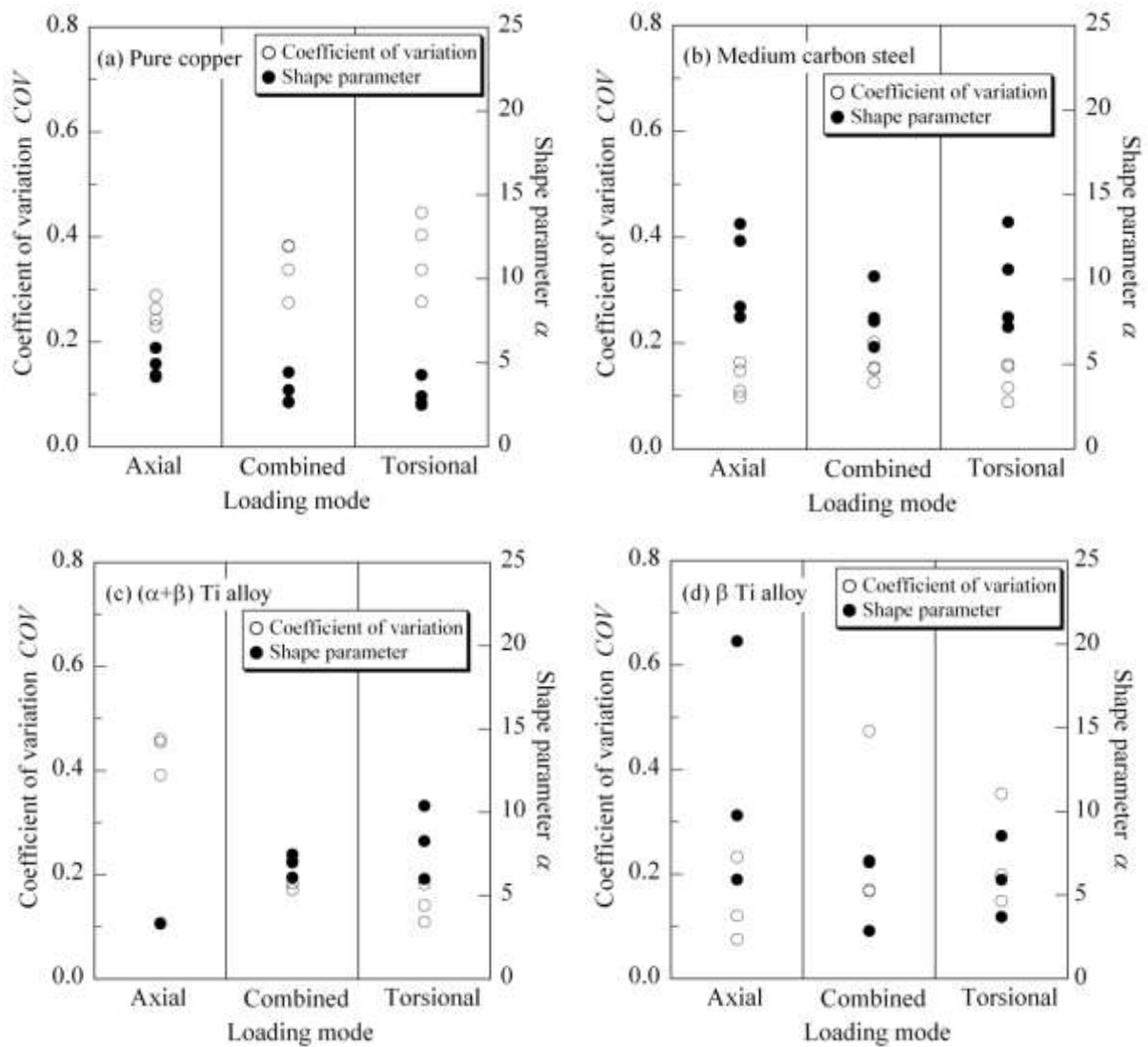


Fig. 9 Coefficient of variation and shape parameter correlated with loading mode